Available online at www.sciencedirect.com
SCIENCE DIRECT
Journal of Sound and Vibration 293 (2006) 599–610
JOURNAL OF SOUND AND VIBRATION
www.elsevier.com/locate/jsvi

Ground vibration due to railway traffic—The calculation of the effects of moving static loads and their experimental verification

L. Auersch*

Federal Institute for Materials Research and Testing, D 12200 Berlin, Germany

Accepted 26 August 2005
Available online 7 February 2006

Abstract

The propagation of waves through homogeneous or layered soil is calculated based on half-space theory. The moving dynamic loads of a train are approximated by fixed dynamic loads and the wave field can be calculated if the spectrum of the dynamic train loads is known. In addition to this dynamic wave field, there are three different components at three different frequency ranges which are caused by the passage of the static loads:

- the regular static component at low frequencies,
- the irregular static component at medium frequencies,
- the sleeper-passing component at high frequencies.

For each of these components, an approximate solution is presented. The calculated wave field is compared with measurements of different trains at different sites. The measurement of impulse and harmonic point load excitation verifies the soil dynamic base of the method.

1. Introduction and methods of calculation

Ground vibration due to railway traffic has quite a number of possible sources. One of these sources is due to the moving static loads of the train which have been analysed for example by Auersch [1], Ford [2], Jones and Block [3], Krylov [4], Sheng et al. [5], and Degrande and Lombaert [6]. In the past, the importance of the moving static load seemed to be overestimated. The purpose of this contribution is to distinguish the different parts of the ground vibration due to the static loads and to find out the importance of each of them by calculation and by measurements, namely by measurements of the trains ICE 3 and Thalys on the Berlin-Hannover high-speed line (Figs. 1 and 2).

In Ref. [7], an exact numerical solution for the wave propagation in homogeneous or layered soil was presented. From the results of this method, a simplified procedure was derived which allows the prediction of the soil vibration due to the dynamic loads of railway traffic. An example prediction is demonstrated in

*Tel: +49 30 8104 3290; fax: +49 30 8104 1727.
E-mail address: lutz.auersch-saworski@bam.de.

0022-460X/$ - see front matter © 2006 Elsevier Ltd. All rights reserved.
doi:10.1016/j.jsv.2005.08.059

Fig. 1. The ICE 3 train at the measurement site, the Berlin–Hannover high-speed line.

Fig. 2. The Thalys train at the measurement site.

Appendix A, where also the basis of the method—the transfer function of the soil—is verified experimentally. The method is now extended to include the soil response to the passage of static loads.

This contribution presents the calculation of

- axle sequence spectra,
- the response to the passage of an axle or a train,
- the effect of scattered axle impulses,
- and the effect of the sleeper passage.

The sleeper-passage effect is also due to the passage of static loads but the ground vibration is generated by dynamic loads caused by the corresponding accelerations of the vehicle. The corresponding method of calculating the vehicle–track–soil interaction was first published in Ref. [1].

2. The axle sequence of trains and the corresponding spectra

The passage of a train consists of a number of similar events, for example displacements $u_0(t)$ with certain delay times T_i

$$u(t) = \sum_{i=1}^{n} u_0(t - T_i). \tag{1}$$

These delay times are related to the distances between the axles of the train and to the speed of the train. When this equation is transformed to the frequency domain according to the rule for a delay time, the spectrum of $u(t)$

$$U(f) = U_0(f) \sum_{i=1}^{n} \mathrm{e}^{-\mathrm{j}2\pi f T_i} =: U_0(f) X(f) \tag{2}$$

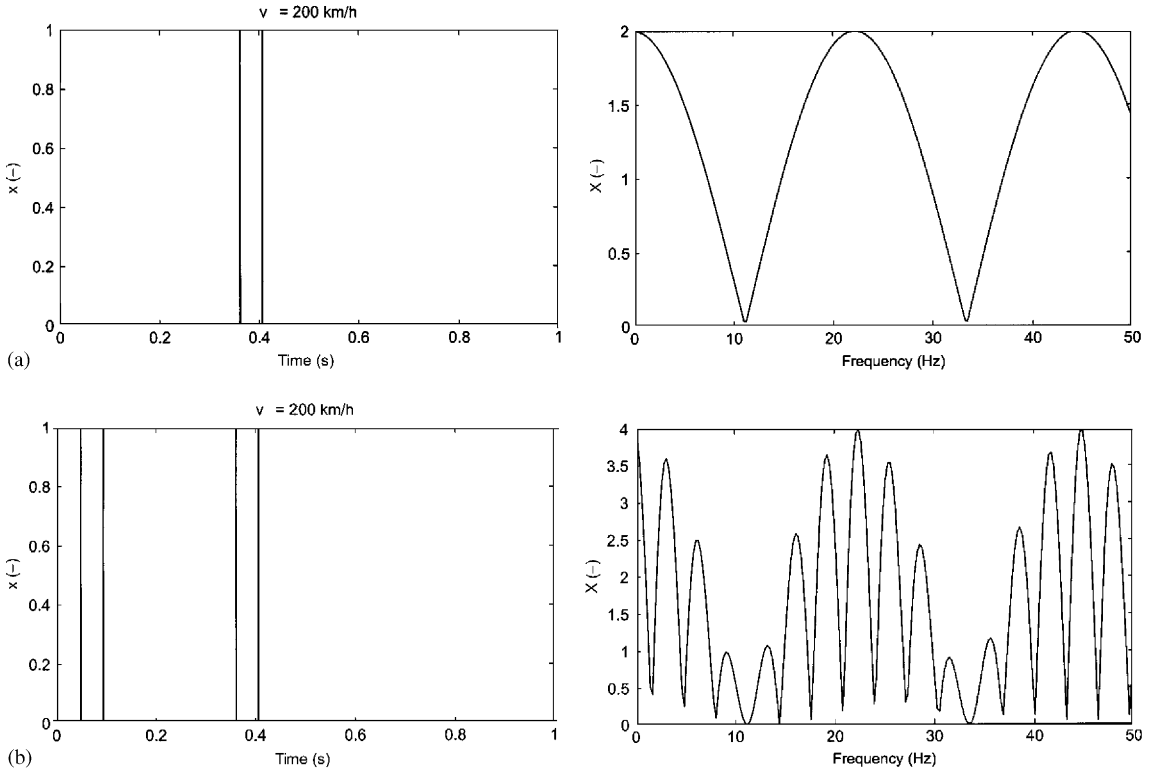

Fig. 3. The axle sequence, time history and spectrum of (a) a bogie and (b) a carriage.

is a product of the displacement spectrum $U_0(f)$ of the single axle and of a dimensionless spectrum $X(f)$ which characterizes the sequence of the axles.

If only two axles (for example of a bogie in Fig. 3a) are considered, the amplitude spectrum is

$$X(f) = 1 + e^{-j2\pi f T} \rightarrow |X(f)| = 2|\cos \pi f T|. \tag{3}$$

This spectrum has maxima at

$$f = 1/T,\ 2/T,\ \ldots,\ n/T, \tag{4}$$

which means that the succession of axles does not prefer a certain frequency region nor are there significant peaks in the spectrum. More characteristically the zeros of the spectrum are at

$$f = 1/2\,T,\ 3/2\,T,\ ...,\ (2n+1)/2T. \tag{5}$$

The zero frequencies remain constant for products of sequence spectra, for example a pair of axles $X_A(f)$ and a pair of bogies $X_B(f)$

$$X(f) = X_A(f) X_B(f). \tag{6}$$

In addition to the two zeros of a bogie (Fig. 3a), a car with two bogies yields a number of narrow-spaced zeros (Fig. 3, bottom). The corresponding time histories $x(t)$ of the axle sequence is represented by finite impulse functions in Figs. 3 and 4.

Next, the axle sequence spectra of complete trains are considered. Fig. 4 shows the spectra of an ICE 3 train and of a Thalys train. Due to the sequence of eight similar carriages of the ICE 3, the spectrum has peaks at a regular spacing of

$$\Delta f = 1/T_C, \tag{7}$$

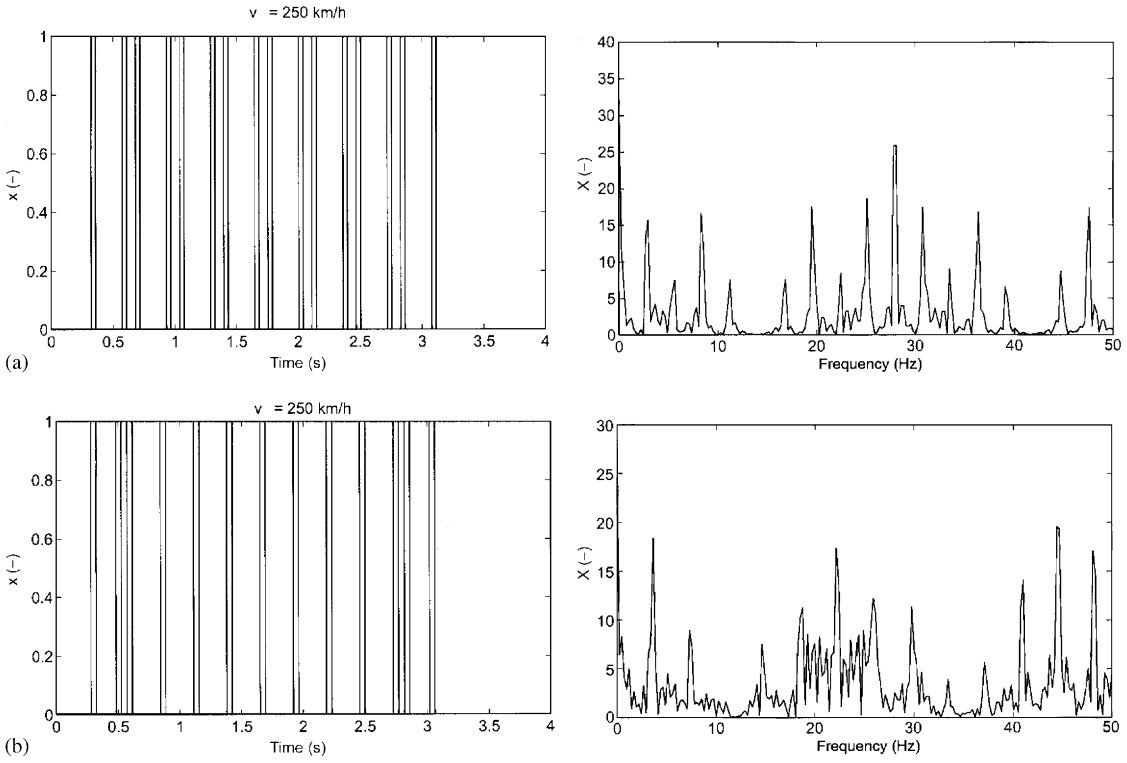

Fig. 4. The axle sequence, time history and spectrum of the (a) ICE 3 and (b) Thalys.

where T_C is the time for the passage of a carriage. Characteristic zeros are at 6, 12.5 and 40 Hz.The Thalys train is formed of two locomotives, two end cars and six carriages, so it yields a more irregular axle sequence spectrum. The Thalys spectrum has a characteristic broad-band region between 16 and 32 Hz.

The same axle sequence spectra could be found in the measurements. Fig. 5 shows the measured velocities of the sleepers during the passage of the ICE 3 and the Thalys.

3. The passage of static loads

The displacements u of the soil due to the passage of one static load P is calculated approximately by using the amplitude–distance law of a homogeneous half-space

$$u \sim 1/r \tag{8}$$

and

$$u(t,x) \sim \frac{1}{r(t,x)} = \frac{1}{\sqrt{x^2 + (y_0 + v_T t)^2}} = u^*(t,x), \tag{9}$$

where x is the distance of the observation point to the track, r is the distance of the load to the observation point, y_0 is the position of the load on the track at time $t = 0$, and v_T is the train speed. These normalized time histories $u^*(t, x)$ are transformed into the frequency domain

$$u^*(t,x) \to u^*(f,x) \tag{10}$$

and normalized velocity spectra $v^*(f, x)$ are formed by

$$v^*(f,x) = \mathrm{i}2\pi f\, u^*(f,x) \tag{11}$$

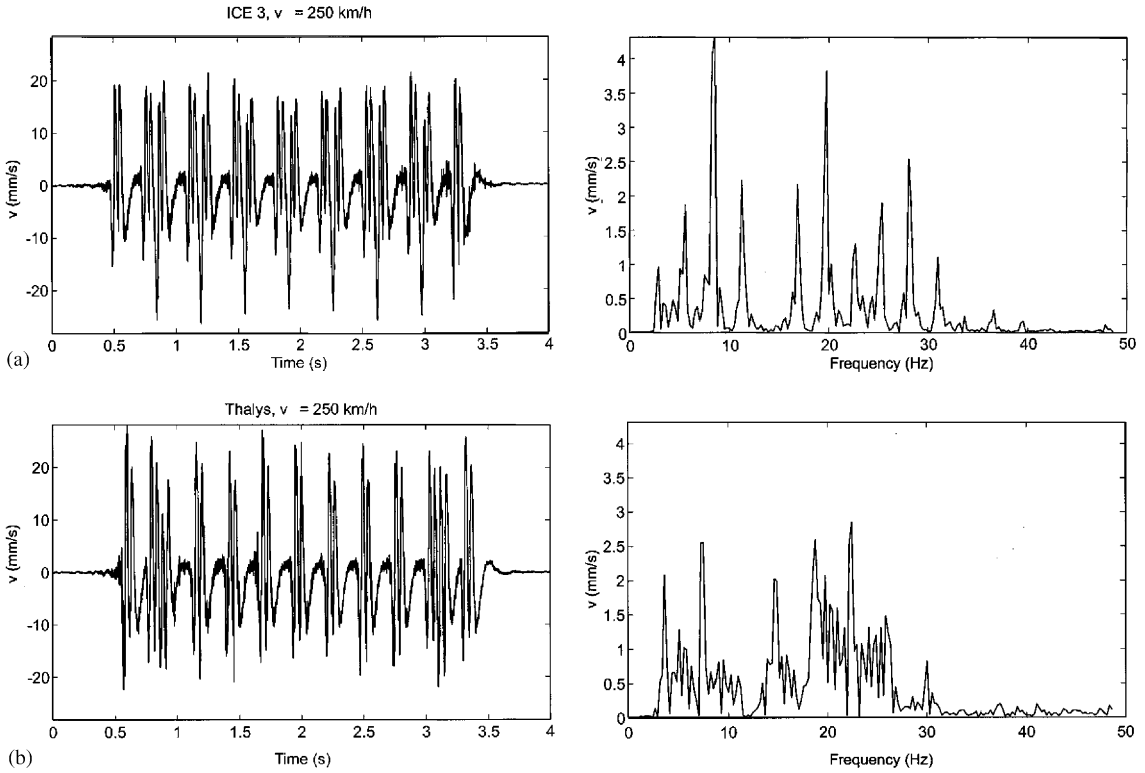

Fig. 5. The measured sleeper velocity, time history and spectrum of the (a) ICE 3 and (b) Thalys.

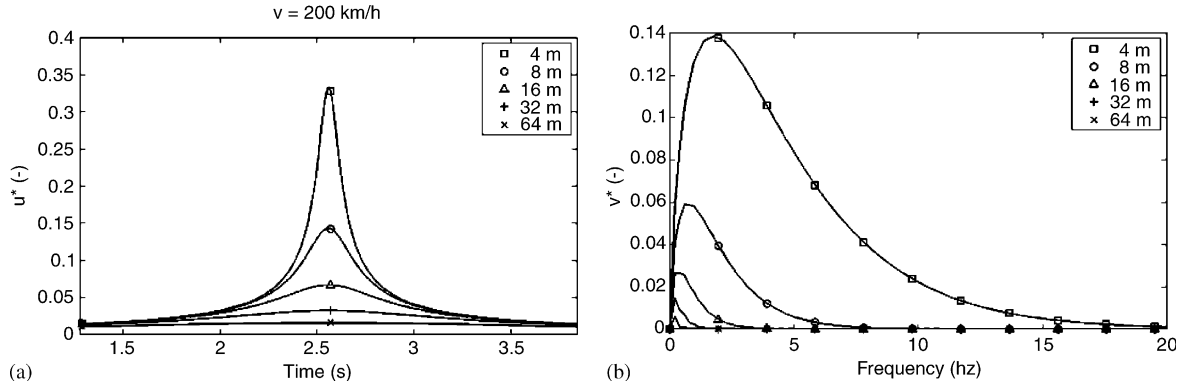

Fig. 6. Normalized soil displacement due to the passage of a static load (a) and the spectrum of the corresponding velocities (b), train speed 200 km/h.

(see Fig. 6). The frequency range of these velocity spectra is restricted to frequencies $f<10$ Hz even for high-speed traffic. The bandwidth of the soil vibration is even smaller if the point of observation is farther from the track.

To get the absolute amplitudes, the normalized amplitudes must be multiplied by the soil parameters (shear modulus G and Poisson ratio v, see Appendix A) and the static force amplitude $P_0 = 150$ kN

$$v(f,x) = \frac{1-v}{2\pi G} v^*(f,x) P_0, \tag{12}$$

see Refs. [8,9]. Finally, the spectrum of one static load is multiplied with the axle sequence spectrum of the train

$$v_{\text{train}}(f,x) = v(f,x)X(f). \tag{13}$$

The results for the ICE 3 and the Thalys are presented in Fig. 7 as one-third octave band spectra. (A small amount of dynamic load ($P_i = 10\,\text{N}$) is added to avoid zero results at higher frequencies.)

The calculated regular static response is compared with the measured amplitudes (Fig. 8). There is a good correlation between the calculated amplitudes and the corresponding low-frequency amplitudes of the measurements. Moreover, the measured differences between ICE 3 and Thalys are well reproduced by the calculation, see for example the higher amplitudes around 4 Hz for the Thalys or the stronger peak at 8 Hz for the ICE 3.

The most important conclusion is that the strong attenuation of the amplitudes due to the passage of static loads is clearly found in theory and experiment. This verification confines the importance of the passage of static loads to the close neighbourhood of the track and to very low frequencies.

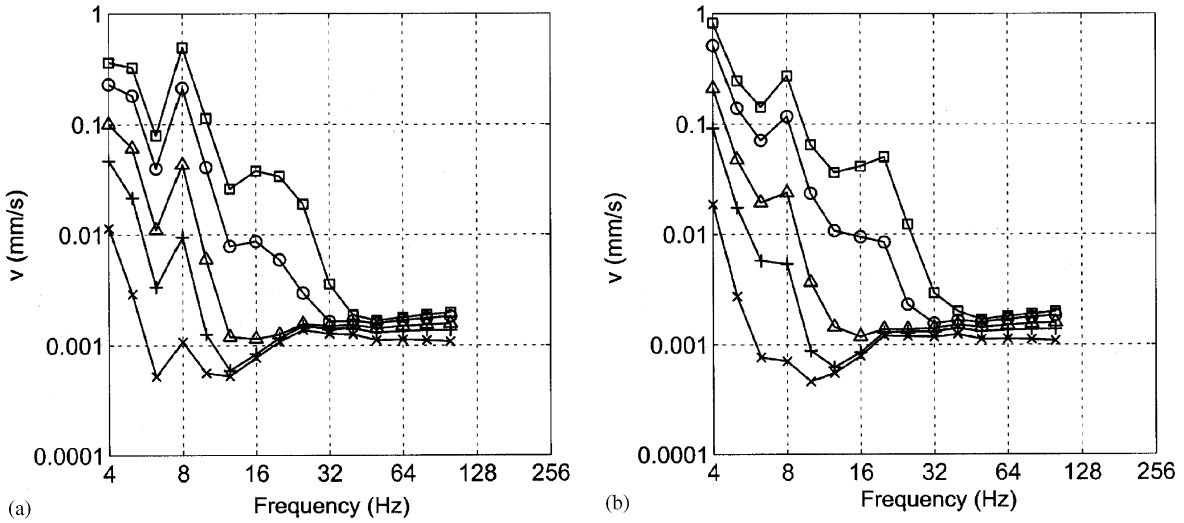

Fig. 7. Passage of the static loads of the (a) ICE 3 and (b) Thalys, amplitudes at □ 3, ○ 4, △ 6, + 8, × 12 m, $v = 250$ km/h.

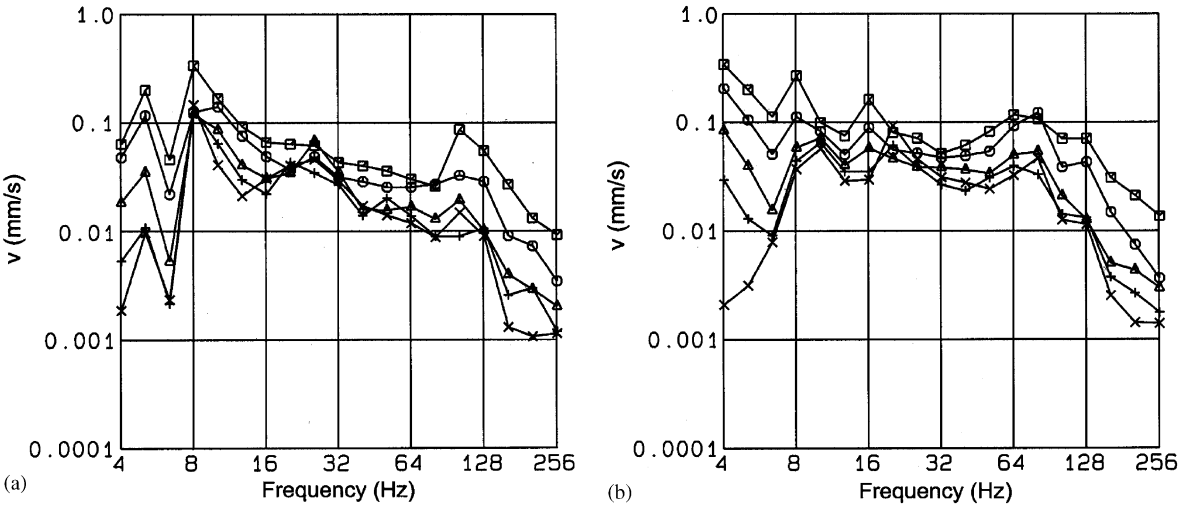

Fig. 8. Measured amplitudes during the passage of the (a) ICE 3 and (b) Thalys, at □ 3, ○ 4, △ 6, + 8, × 12 m, $v = 250$ km/h.

4. The passage of static loads over a soil with randomly varying properties

One part of the ground vibration can be caused by irregularities of the soil. This hypothesis is based on a number of experimental observations.

- Huber [10] first observed that the ground vibrations of two different passages of ICE trains with the same speed are almost identical whereas the ground vibrations at a measurement line a few metres ahead were completely different from those of the first measurement line. These observations were explained by assuming a soil with a spatial variation of the wave speed [10].
- The axle sequence spectrum of an ICE test train was clearly found in the ground vibrations at a measurement site near Würzburg [11]. The frequency content was considerably higher than for the regular static component, which could be identified by its strong attenuation with distance and frequency. It was concluded that only a soil with randomly varying properties can be the cause of this observation [11].
- Later, the irregularities of the soil have been measured at this measurement site near Würzburg. The ground vibrations due to an impulse 5 m to the left of the measurement line (Fig. 9a) were compared with those due to an impulse 5 m to the right (Fig. 9b). The amplitude spectra are very similar as expected for a regular soil. But if the difference of the complex transfer functions is built, a considerable portion of the impulse spectrum is left over—the scatter of the impulse (Fig. 9c).

A simple method is established which directly describes these measured effects without any specific random soil model. The basic idea is that the impulses on different sleepers generate two different parts of the ground vibration. The main contribution consists of the regular responses which are similar for different sleepers and result in a quasi-static motion of the soil as discussed in the previous section. A small part of the impulses of

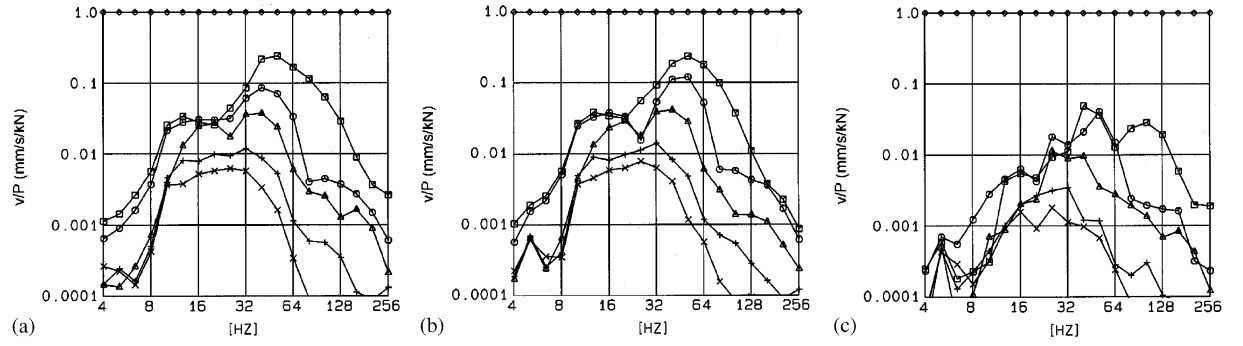

Fig. 9. Scattering of impulses due to irregularities of the soil. Soil amplitudes at □ 5, ○ 7, △ 17, + 37, × 62 m from the impulse (a) 5 m left and (b) 5 m right of the measuring line and (c) difference of both excitations.

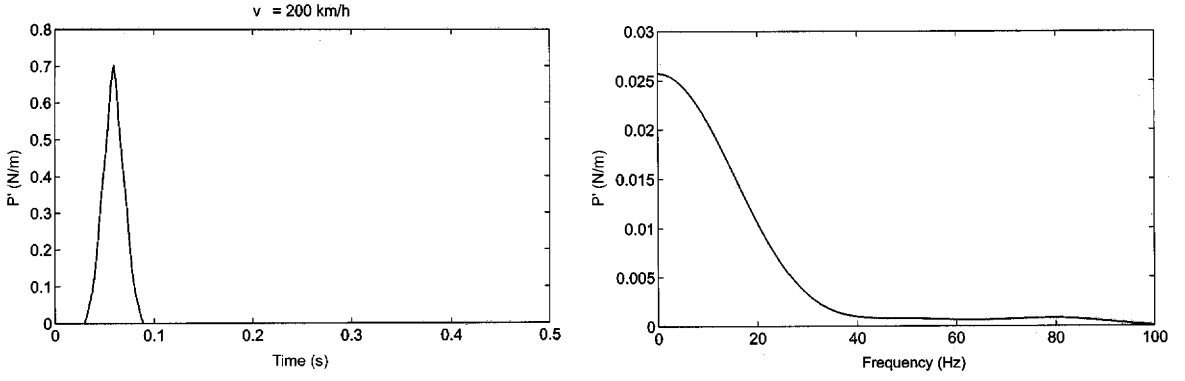

Fig. 10. Impulse load of one axle with $P = 1$ N and $v = 200$ km/h, time history and spectrum.

different sleepers is scattered due to the randomly varying soil properties. This contribution is apparent in the ground vibration with its original higher-frequency content.

To get a first approximation of this irregular part of the ground vibration, the distribution of the axle load along the track $p'(y)$ or with time $p'(t) = p'(y = v_T t)$ is calculated first (Fig. 10). This distribution gives the impulse of the passage of one axle and the corresponding spectrum $P'(f)$. For one sleeper, the impulse is $dP'(f)$ with the sleeper distance d. The scattered part of this impulse is a certain proportion q of the impulse $qdP'(f)$. As the scattering of the impulse response is different for each sleeper, the scattered responses of all n_S sleepers that are excited by one axle during the passage of the train have to be added stochastically as $\sqrt{n_S}qdP'(f)$. Multiplication with the axle sequence spectrum $X(f)$ yields the scattered impulse spectrum P_S of the whole train. The final approximate formula for the scattered impulses is therefore

$$P_S(f) = \sqrt{n_S}qdP'(f)X(f), \tag{14}$$

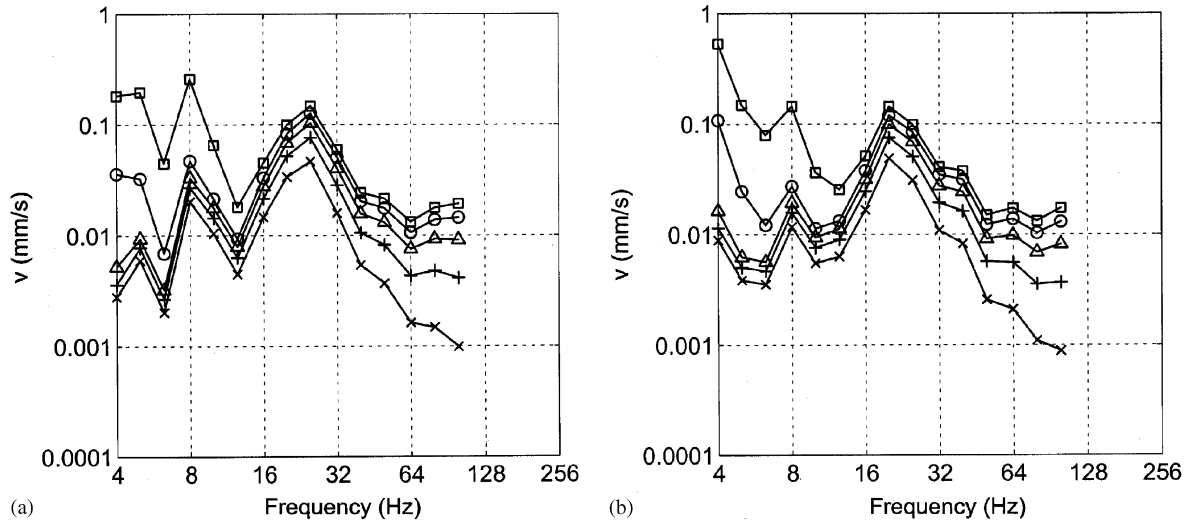

Fig. 11. Soil amplitudes at □ 4, ○ 8, △ 16, + 32, × 64 m due to the scattering of impulses ($q = 3\%$) and the regular static part (a) ICE 3 and (b) Thalys, $v = 250$ km/h.

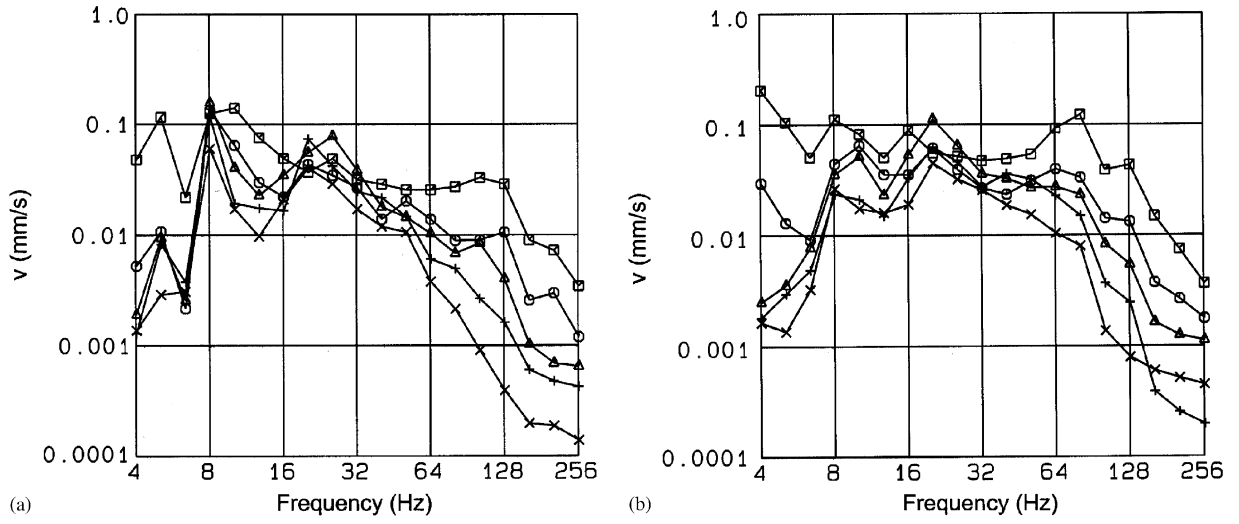

Fig. 12. Measured amplitudes at □ 4, ○ 8, △ 16, + 32, × 64 m during the passage of the (a) ICE 3 and (b) Thalys, $v = 250$ km/h.

where q is the proportion of the scatter, d is the sleeper distance, $n_S = L_T/d$ is the number of the sleepers, $P'(f)$ is the load spectrum (force per length), and $X(f)$ is the axle sequence. The corresponding ground vibration is then calculated with the transfer function given in Appendix A.

This procedure is used to calculate the passage of the ICE 3 and the Thalys with $v = 250$ km/h. A scatter of $q = 3\%$ is used, and the regular static contribution is calculated, too. In Fig. 11, the irregular static component displays completely different characteristics compared with the regular static component of the preceding section. The irregular component is increasing with frequency while the regular component is mainly decreasing with frequency. In addition, the attenuation with distance is much stronger for the regular static component. So the irregular static component can clearly be identified. Its highest amplitudes are between 16 and 32 Hz, but also the peak at 8 Hz is due to the scattering part—at least at the far-field points. Corresponding results are shown for the measurement in Fig. 12. The measured soil amplitudes are almost at the same level as for the calculation, only the high-frequency amplitudes are higher than the calculated irregular static component. The measured attenuation with distance may be weaker than calculated at some frequencies.

So it can be concluded that the scattering of the axle impulses due to the varying properties of the soil can explain an important mid-frequency part of the ground vibration. The completely different attenuation of the regular part makes it clear that the regular static component cannot be present in that mid-frequency range.

The higher measured amplitudes between 50 and 125 Hz are due to irregularities of the vehicle and the track such as rail roughness and out-of-round wheels. Moreover, the vehicle–track resonance, which amplifies any dynamic excitation, typically lies in this frequency region [12,13]. Another dynamic load, which is analysed in the next section, is due to the sleeper passage. The corresponding sleeper-passage frequency can clearly be found in the measured results at 125 Hz.

5. The passage of static loads over a track with equally spaced sleepers

The main effect of the sleeper passage is the corresponding up and downward motion of the unsprung mass of the vehicle and the additional dynamic load of a track due to that motion. The dynamic forces are calculated solving the complete vehicle–track–soil interaction [12]. The solution can be given approximately as

$$P_1(f_S) = K_V(f_S)\frac{K(0)}{K(f_S)}\frac{u_S}{2}, \tag{15}$$

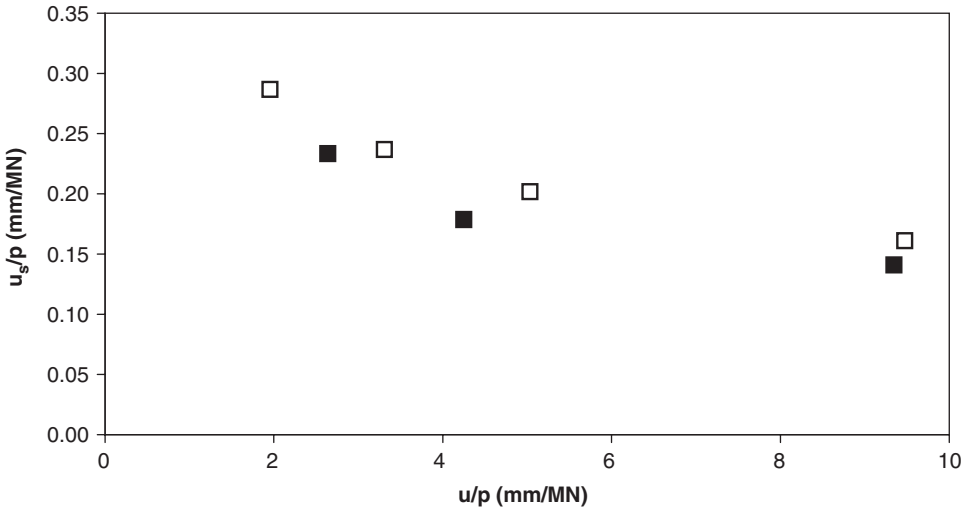

Fig. 13. Secondary displacement u_s of the rail between two sleepers as a function of the primary displacement u, variation of the stiffness of the rail pad ■ and the soil □.

where P_1 is the force due to the sleeper passage, f_S is the sleeper-passage frequency, K_V is the dynamic stiffness of the vehicle, $K = K_V + K_T$ is the dynamic stiffness of the vehicle and track system, and u_S is the secondary displacement of the rail between two sleepers. The secondary as well as the primary displacement u_S of the rail is calculated for a number of different tracks with UIC 60 rail and concrete sleepers at a distance of $d = 0.6$ m, on four different soils (with shear wave speed $v_S = 100$, 150, 200, 300 m/s) and with three different rail pads (with pad stiffness $k_P = 20$, 80, 300 kN/mm). The primary displacements are between $u/p = 2 \ldots 10$ mm/MN, where high compliance is possible for soft soil or soft rail pads [9]. The secondary displacements of both variations are presented in Fig. 13 as a function of the primary displacement. The stiffness of the track has an influence on the secondary displacement u_S. A softer track yields a smaller u_S, where the soft rail pads give a little bit smaller values than a comparable soft soil. The shear deformation of the rail—included by a shear area of 40% of the cross-section—gives a considerable contribution to the secondary displacement.

The frequency-dependent transfer function for the sleeper-distance load according to the preceding formula is calculated for different soil stiffnesses and presented in Fig. 14. The main finding is that the dynamic sleeper-passage force increases with the train speed up to the point where the sleeper-passage frequency reaches the

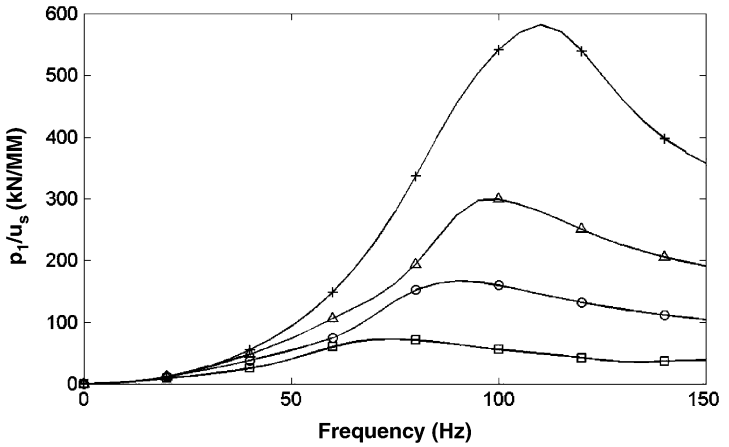

Fig. 14. Transfer function of the dynamic sleeper-passage load p_1 to the secondary displacement u_s, variation of the soil $v_S = \square$ 100, ○ 150, △ 200, + 300 m/s.

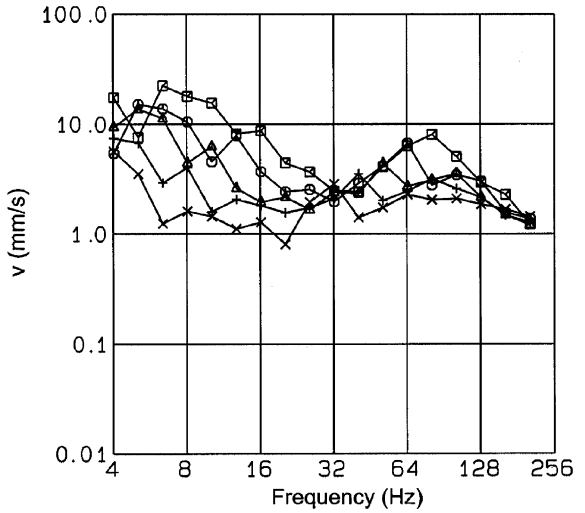

Fig. 15. Measured velocity of the wheelset at train speed of × 63, + 80, △ 100, ○ 125, □ 160 km/h, sleeper-passage frequency at × 32, + 40, △ 50, ○ 64 and □ 80 Hz.

vehicle–track eigenfrequency. For higher frequencies or train speeds, the force does not continue to increase or even decreases. The theoretical results could be verified by measurements of the test runs of the ICE [1]. Because of the very good condition of the test train and the newly built track, the sleeper-passage part was clearly separated from the other source components and could be analysed in detail. Later measurements under normal conditions—with considerable out-of-round wheels—showed once again the dominant dynamic loads due to sleeper passage, see Ref. [14] and Fig. 15.

6. Conclusion

The role of the static loads in the ground vibration near railway lines is analysed. Three completely different parts of excitation are distinguished: the regular static part, the irregular static part (due to the scattering of the axle impulses) and the regular dynamic part (due to the sleeper passage). It is shown by calculation and by measurement that the regular static part—sometimes called the quasi-static part—is of importance only at very low frequencies at the near-field of the track.

In general, the ground vibration near railway lines is caused by dynamic loads due to irregularities of the vehicle and track or due to the regular track variation with sleeper-distance frequency. In addition, the scattering of the axle impulses by a randomly varying soil seems to be of importance. For the high-speed tests, a small amount of scatter could explain the main part of the measured ground vibration.

Appendix A. Details of the measured soil and the prediction for dynamic train loads

The soil at the measuring site was investigated by means of an impulse and a harmonic vibrator excitation. The wave speed of the soil was determined by a delay-time measurement resulting in a shear wave speed of $v_S = 170\,\mathrm{m/s}$. The material damping of the soil was established from the amplitude–distance law as $D = 1\%$. Moreover, the measurements with the impulse and the harmonic excitation were used to construct the transfer function of the soil (Fig. 16). The transfer functions are nearly the same for both types of excitation. They also agree well with the theoretical transfer function of a homogeneous soil with $v_S = 170\,\mathrm{m/s}$ and $D = 1\%$ which is shown in Fig. 17a.

Fig. 17b shows the prediction of the train-induced vibration with an assumed dynamic load of $P_i = 1\,\mathrm{kN}$ for each one-third-octave band and each of the 40 axles along the length $L_T = 250\,\mathrm{m}$ of the train. The superposition of a number of axle loads yields higher amplitudes than a single load especially at far-field

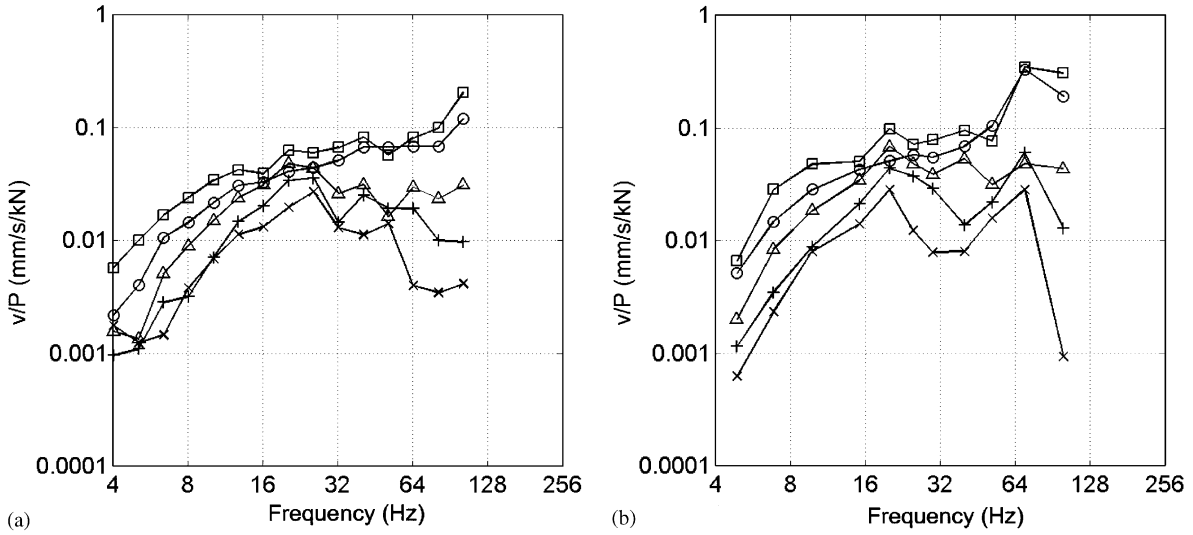

Fig. 16. Transfer function of the soil at □ 4, ○ 8, △ 16, + 32, × 64 m, measured with (a) impulse excitation and (b) harmonic vibrator excitation.

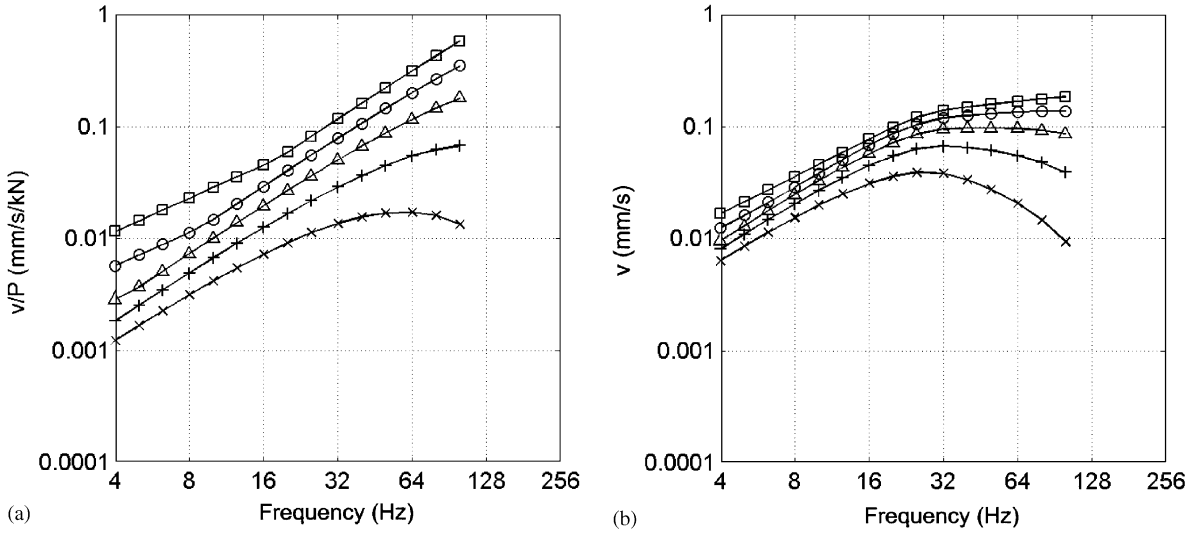

Fig. 17. Predicted amplitudes of the soil with $v_S = 170\,\mathrm{m/s}$ and $D = 1\%$, (a) point load with $P = 1\,\mathrm{kN}$ (transfer function) and (b) dynamic train load (40 axle loads with $P = 1\,\mathrm{kN}$ along $L_T = 250\,\mathrm{m}$), at □ 4, ○ 8, △ 16, + 32, × 64 m.

points. For high frequencies, there is a second but opposite effect for a train load. As each axle load is distributed across the track, there is a reduction for the high frequency and short wavelength vibration. The predicted amplitudes could be used as a rough first approximation of the measured ground vibration caused by the ICE 3 and Thalys (Fig. 12).

References

[1] L. Auersch, Zur Entstehung und Ausbreitung von Schienenverkehrserschütterungen: theoretische Untersuchungen und Messungen am Hochgeschwindigkeitszug Intercity Experimental, *BAM-Forschungsbericht* 155 (1988).
[2] R.A.J. Ford, Track and ground vibrations from trains running on conventional ballasted track, *Proceedings of the Institution of Mechanical Engineers/ Rail and Rapid Transit* 206 (1992) 117–126.
[3] C.J.C. Jones, J.R. Block, Prediction of ground vibration from freight trains, *Journal of Sound and Vibration* 193 (1996) 205–213.
[4] V. Krylov, Effects of track properties on ground vibrations generated by high-speed trains, *Acustica-Acta Acustica* 84 (1998) 78–90.
[5] X. Sheng, C.J.C. Jones, M. Petyt, Ground vibration generated by a load acting along a railway track, *Journal of Sound and Vibration* 228 (1999) 129–156.
[6] G. Degrande, G. Lombaert, High-speed train induced free-field vibrations: in situ measurements and numerical modelling, in: N. Chouw, G. Schmid (Eds.), *Proceedings of the WAVE 2000*, A.A. Balkema, Rotterdam, 2000, pp. 29–42.
[7] L. Auersch, Wave propagation in layered soil: theoretical solution in wavenumber domain and experimental results of hammer and railway traffic excitation, *Journal of Sound and Vibration* 173 (1994) 233–264.
[8] H. Lamb, On the propagation of tremors over the surface of an elastic solid, *Philosphical Transactions of Royal Society A* (London) 203 (1904) 1–42.
[9] L. Auersch, The excitation of ground vibration by rail traffic: theory of vehicle–track–soil interaction and measurements on high-speed lines, *Journal of Sound and Vibration* 284 (2005) 103–132.
[10] G. Huber, Erschütterungsausbreitung beim Rad/Schiene-System, Dissertation, Universität Karlsruhe, 1988.
[11] L. Auersch, Fundamentschwingungen und Wellenausbreitung bei inhomogenen Böden—Beiträge zur Dynamik der Verkehrssysteme, *BAM-Forschungsbericht* 226 (1998).
[12] L. Auersch, Zur Parametererregung des Rad-Schiene-Systems: Berechnung der Fahrzeug-Fahrweg-Untergrund-Dynamik und experimentelle Verifikation am Hochgeschwindigkeitszug Intercity Experimental, *Ingenieur-Archiv* 60 (1990) 141–156.
[13] M. Heckl, G. Hauck, R. Wettschureck, Structure-borne sound and vibration from rail traffic, *Journal of Sound and Vibration* 193 (1996) 175–184.
[14] L. Auersch, S. Said, W. Rücker, Das Fahrzeug-Fahrweg-Verhalten und die Umgebungserschütterungen bei Eisenbahnen, *BAM-Forschungsbericht* 243 (2001).